ORIGINAL RESEARCH

Synthesis and evaluation of *ortho*-[18F] fluorocelecoxib for COX-2 cholangiocarcinoma imaging

Chi-Wei Chang[1],*
Chun-Nan Yeh[2],*
Yi-Hsiu Chung[3],*
Yong-Ren Chen[4]
Shi-Wei Tien[4]
Tsung-Wen Chen[2]
Shiou-Shiow Farn[4,5]
Ying-Cheng Huang[6]
Chung-Shan Yu[4,7]

[1]Department of Nuclear Medicine, Taipei Veterans General Hospital, Taipei, Taiwan; [2]Department of Surgery, Liver Research Center, Chang-Gung Memorial Hospital at Linkou, Chang Gung University, Taoyuan, Taiwan; [3]Center for Advanced Molecular Imaging and Translation, Chang Gung Memorial Hospital, Taoyuan, Taiwan; [4]Department of Biomedical Engineering and Environmental Sciences, National Tsinghua University, Hsinchu, Taiwan; [5]Isotope Application Division, Institute of Nuclear Energy Research, Taoyuan, Taiwan; [6]Department of Neurosurgery, Chang-Gung Memorial Hospital at Linkou, Chang Gung University, Taoyuan, Taiwan; [7]Institute of Nuclear Engineering and Science, National Tsinghua University, Hsinchu, Taiwan

*These authors contributed equally to this work

Correspondence: Chung-Shan Yu
Department of Biomedical Engineering and Environmental Sciences, National Tsinghua University, Hsinchu 300, Taiwan
Email csyu@mx.nthu.edu.tw

Background: An 18F-tagged NSAID analog was prepared for use as a probe for COX-2 expression, which is associated with tumor development.

Methods: The in vivo uptake of celecoxib was monitored with *ortho*-[18F]fluorocelecoxib using positron emission tomography (PET). The binding affinity of *ortho*-[18F]fluorocelecoxib to COX-1 and COX-2 enzymes were assessed using the competitor celecoxib.

Results: The IC_{50} values were 0.039 μM and 0.024 μM, respectively. A selectivity index of 1.63 was obtained (COX-2 vs COX-1). COX-2 overexpressed cholangiocarcinoma (CCA) murine cells took up more *ortho*-[18F]fluorocelecoxib than that by usual CCA cells from 10 to 60 minutes post incubation. Competitive inhibition (blocking) of the tracer uptake of *ortho*-[18F]fluorocelecoxib in the presence of celecoxib by the COX-2 overexpressed CCA cells and the usual CCA cells gave the IC_{50} values of 0.5 μM and 46.5 μM, respectively. Based on the in vitro accumulation data and in vivo metabolism half-life (30 min), PET scanning was performed 30–60 min after the administration of *ortho*-[18F]fluorocelecoxib through the tail vein. Study of *ortho*-[18F]F-celecoxib in the CCA rats showed a tumor to normal ratio (T/N) of 1.38±0.23 and uptake dose of 1.14±0.25 (%ID/g).

Conclusion: The inferior in vivo blocking results of 1.48±0.20 (T/N) and 1.18±0.22 (%ID/g) suggests that the nonspecificity is associated with the complex role of peroxidase or the binding to carbonic anhydrase.

Keywords: celecoxib, fluorination, imaging, NSAIDs, blocking, PET

Introduction

Cholangiocarcinoma (CCA) is a type of liver cancer that occurs in the epithelial lining of the biliary tract. Globally, it is the second most rapidly increasing malignant liver tumor.[1–3] Although surgical resection is an effective treatment for CCA,[4–6] the patient survival ratio remains very poor. The unmet medical needs for CCA include diagnosis at advanced stage, dismal prognosis leading to death of the patients within 1 year,[7] and resistance to traditional chemotherapy and radiotherapy.

Recent studies have indicated that local inflammation around the biliary tree was highly associated with the epithelial transformation of the biliary tract from dysplasia to malignancy.[8,9] The enzyme cyclooxygenase (COX) is crucial in such inflammatory cascades because it can catalyze the conversion of arachidonic acid to prostanoids.[10] The inducible COX-2 enzyme is expressed in some human CCA cell lines upon inflammation.[11–13] In contrast, the homeostatic COX-1 enzyme, a housekeeping enzyme, regulates gastric acid in gastric mucosa. Therefore, COX-2 inhibitors or COX-2-specific binding compounds are considered reasonable targets for cancer therapy. The nonsteroidal anti-inflammatory drug (NSAID) such as aspirin has been reported to be

inversely associated with the development of CCA. However, the biologic mechanism underlying prevention of CCA is plausible, especially by the COX-2 inhibitor.[14] Although chronic use of high doses of selective COX-2 inhibitors such as coxibs, rofecoxib, and valdecoxib was associated with increased cardiovascular risk, celecoxib is still in use owing to an improved safety profile (Figure 1). Nevertheless, as COX-2 overexpression is associated with poor prognosis, celecoxib may still be of value for short-term treatment of COX-2-expressing tumors as a single drug or in combination with classic chemotherapeutic drugs or radiotherapy.[15]

The diagnosis tool positron emission tomography (PET) imaging provides metabolic information on drugs that have been tagged with second-period isotopic atoms, for example, ^{11}C, ^{13}N, ^{15}O, and ^{18}F. The introduction of an ^{18}F atom moderately alters parent structure owing to its similar Van der Waals radius as hydrogen.[16] Thus, the physiologic function of the parent compound can be retained. ^{18}F is a positron emitter ($t_{1/2}$=109.7 min; β^+, 99%) with a coherent calibrating feature that can be coupled with PET to perform quantitative analysis, which is a unique characteristic among the current clinical imaging systems. PET imaging provides superior temporal and spatial resolution compared with single photon emission tomography and allows deduction of the concentration profile of the desired compound. ^{18}F with an appropriate half-life has been labeled in celecoxib at different positions (Figure 1). However, there were a number of difficulties rendering the biologic results such as rapid in vivo defluorination **2–4**,[17–19] unsuccessful in vivo blocking results **5**,[20,21] and lower specific binding affinity **6**.[22] ^{11}C-Labeled celecoxib analogs **7**, **8** were more metabolically stable in vivo owing to the presence of *ortho*-fluoro group to resist its metabolism to form the carboxylic group.[23,24] However, instead of a diaza five-member ring, the structurally altered imidazole ring may bias the molecular recognition. Other structural variation includes substitution of an *ortho*-chloro substituent for a *meta*-trifluoromethyl group. In addition, the short half-life of ^{11}C may not be suitable for tracing longer metabolism. With respect to the pharmacokinetics that can timely evaluate a potential candidate molecule discovered from library screening, prompt tagging of ^{18}F on this parent molecule would be meaningful. Hence, we are interested in preparing
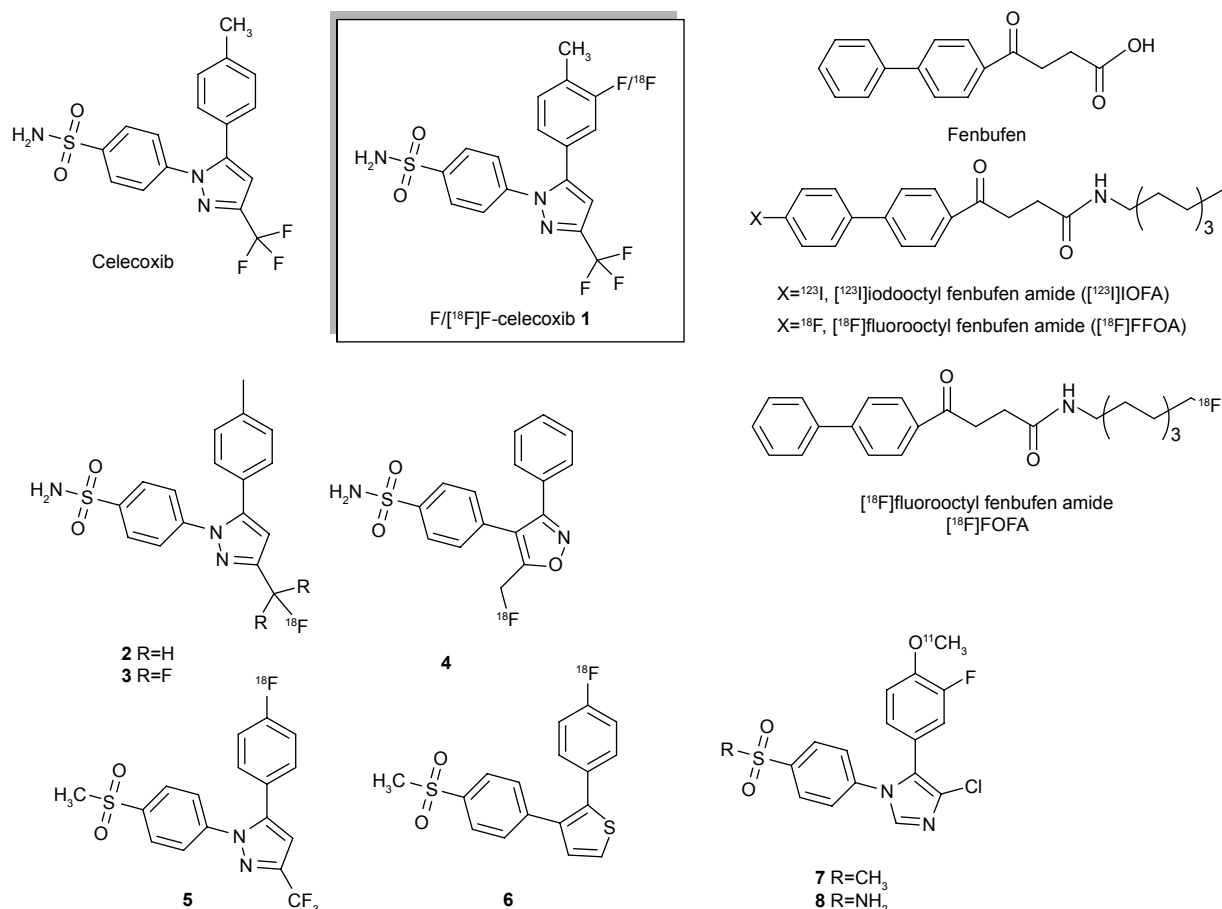

Figure 1 Structures of the target compound *ortho*-F-celecoxib **1**, the reported celecoxib, fluorolabeled celecoxib **2**, **3**, and other tagged NSAID analogs.
Abbreviation: NSAID, nonsteroidal anti-inflammatory drug.

a fluoro-labeled celecoxib through a facial fluorination without changing structure. Compared with the nucleophilic fluorination that requires a tedious procedure for preparing the precursor, electrophilic radiofluorination on an arom ring of parent molecule is more straightforward. The in vivo PET imaging profile generated by tagged COX-2 inhibitors such as [¹⁸F]F-celecoxib could describe the affinity of celecoxib toward cancer; this information would be useful for quick assessment of its clinical potency.

Results and discussion
Preparation of *ortho*-[¹⁸F]F-celecoxib, [¹⁸F]F-I

Electrophilic fluorination using $CF_3COO[^{18}F]F$ is a practical and rapid method for the introduction of ^{18}F atom into celecoxib (Figure 2).[25]

The radiofluorination of celecoxib using a fluorine gas mixture of [¹⁸F]F_2 and F_2 produced the mixture of *ortho*-[¹⁸F]F-**1**, which could be primarily purified using high-performance liquid chromatography (HPLC; Figure 3). The radiochemical yield of the obtained fluorinated product *ortho*-[¹⁸F]F-**1** was 9%. After the radioactive decay of ^{18}F, the cold counterpart *ortho*-^{19}F-**1** was analyzed spectroscopically. A parallel cold fluorination was conducted with CH_3COOF to generate *ortho*-F-**1** for further spectroscopic comparison. The structures and purities were identified using nuclear magnetic resonance (NMR) and mass spectrometry. All the tagged samples were purified using preparative HPLC for the bioassays. However, the fluorination was not effective for the arom *trans*-resveratrol, a selective COX-1 inhibitor. It should be more reactive than celecoxib because of the electron-donating effect by the hydroxyl group. However, the relatively less reactive intermediate CF_3COOF rather than the more reactive CH_3COOF may address this result (Figure 2B).

Tagged ligand-binding study

A common binding assay for COX is based on the inhibition of the conversion of a ^{14}C-labeled arachidonic acid to a ^{14}C-prostanoid metabolite in the presence of competitors (Table 1). The binding assay for celecoxib was conducted by Uddin et al,[19] who reported IC_{50} values of >4 and 0.03 µM for COX-1 and COX-2, respectively. An indirect enzyme-linked immunosorbent assay of PGE2 formation resulted in IC_{50} values of 3.7 µM (COX-1) and 0.06 µM (COX-2).[26] Fenbufen analog is one of the NSAIDs and can be easily radiolabeled with isotopes for studying direct binding assay. Hence, the existing data from fenbufen analogs using direct binding and indirect binding assay can be compared with that of celecoxib. Their IC_{50} values are shown in Table 1.[27] Direct assessment of the substrate–enzyme formation is relatively uncommon.[28,29] Previous assay of the binding affinity (K_d) was performed with HPLC coupled with a gel filtration column. The tagged ligand–enzyme binding complex was differentiable from the free ligand.[30,31] Because of the limited aqueous solubility of *ortho*-[¹⁸F]F-**1**, it was not suitable to use reversed-phase HPLC for binding study. Hence, a nonpolar liquid phase and a polar solid support, for example, silica cartridge, were employed to redistribute the polar tagged ligand–COX molecule and the nonpolar ligand (Figure 4).[32] Through the nonlinear regression fit, the IC_{50} values of *ortho*-[¹⁸F]F-**1** were determined to be 39.0 and 24.5 nM for COX-1 and COX-2, respectively. Our results showed a relatively inferior COX-2 selectivity (1.63) compared with the data from other groups. Interestingly, one of the direct binding assays using [³H]celecoxib gave a similar selectivity index of 1.79. The conformation of binding pocket of COX may vary when catalyzing. Direct binding assay measures an intimate contact with the active site. By contrast, the indirect binding assay measures
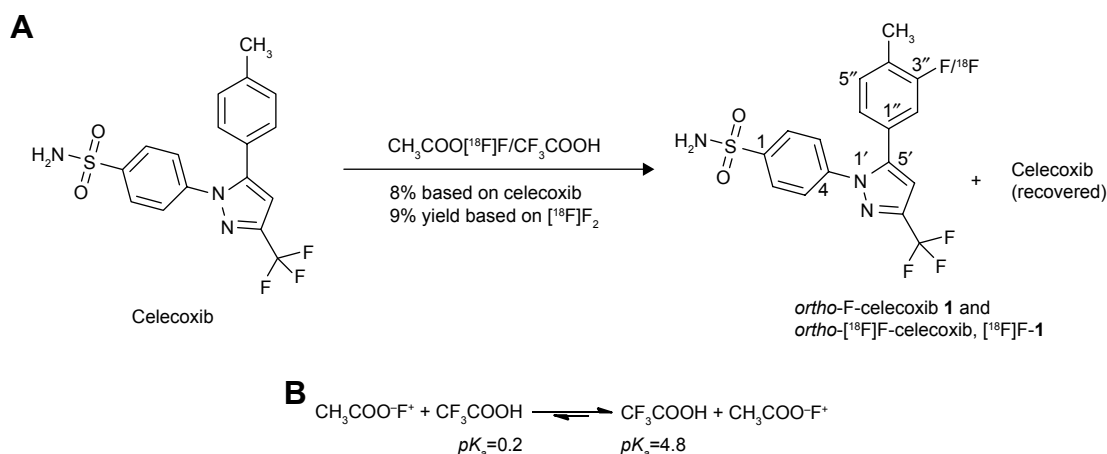

Figure 2 (**A**) Preparation of *ortho*-F-**1**. (**B**) The less reactive CF_3COOF was formed as the major fluorinating reagent.
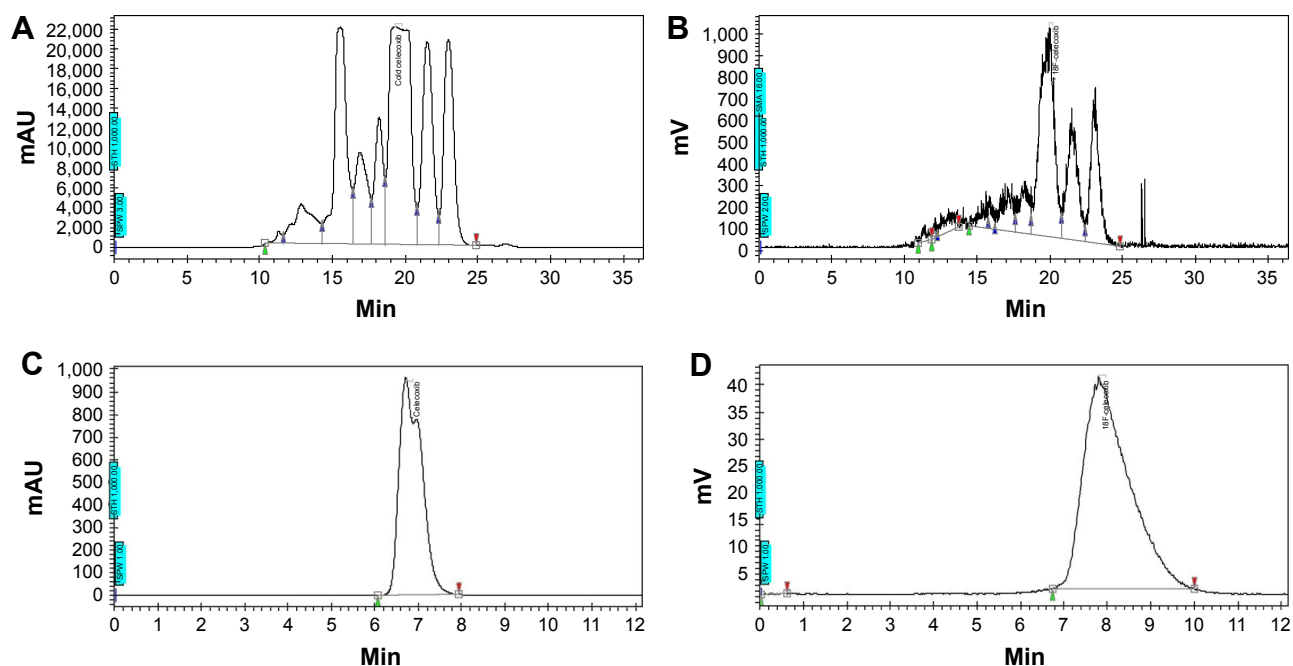
Figure 3 The product mixtures obtained from the radiofluorination of *ortho*-[18F]F-**1** were profiled using high-performance liquid chromatography as shown in the UV– (**A**) and radiochromatograms (**B**).

Notes: The fraction collected from t_R of 19.97 min of the radiochromatogram was identified as *ortho*-[18F]F-**1**. Elution conditions: isocratic mode, RP-18 column, 70% EtOH (aq.), 3 mL/min flow rate, λ=254 nm. The isolated fraction was further confirmed using an analytic high-performance liquid chromatography system as shown in (**C**) UV– and (**D**) radiochromatogram. For clarification, an authentic celecoxib was added to the isolated fraction. The peak at t_R of 7.80 min corresponds to a radiochemical purity of 99.92%. Elution conditions: isocratic mode, RP-18 column, 70% EtOH (aq.), 0.5 mL/min flow rate, λ=254 nm.

the whole function involving the sequential catalysis from COX to peroxidase. Thus, the variable conformation may accommodate the substrate binding. COX-2 is better than COX-1 in tuning the active site for celecoxib analogs.

In vitro tracer accumulation study

The binding affinity of the tracer *ortho*-[18F]F-**1** was also assessed using the COX-2-overexpressed CCA cells[33] and the usual CCA cells. The methods for preparing COX-2-overexpressed cell line have been reported before.[34] The accumulation profiles of the two cells were different in the time course between 10 and 60 min (Figure 5). Hence, this temporal information was incorporated to the subsequent

in vitro blocking study. The quick decline of the tracer uptake after 30 min may be due to the lipophilic metabolite resulting in a quick equilibrium across the cell membrane.

In vitro cellular binding study

Because the binding affinity of Coxibs to tumor cells is mainly challenged by their nonspecific binding to carbonic anhydrase, in vitro blocking study of *ortho*-[18F]F-**1** was carried out to clarify its interaction specificity. The tracer accumulation by the COX-2-overexpressed cell was expected to vary upon the addition of the competitor of celecoxib with various concentrations. Thus, the two competitive inhibition profiles for the two cells were obtained (Figure 6).

Table 1 Binding data obtained from this study and the literature

| Classification	Compound	IC$_{50}$ (µM)		Selectivity index
		COX-1	**COX-2**	
Direct binding assay	[18F]F-FBPin[32]	0.91±0.68	0.33±0.24	2.76
	ortho-[18F]F-**1**	0.039	0.024	1.63
	[3H]celecoxib (K_d)[28,29]	>3.4×10^{-3}	1.9×10^{-3}	>1.79
		15	0.04	375
Indirect binding assay	Fenbufen[27]	3.9	8.1	0.48
	Celecoxib/14C-arachidonic acid	>4	0.03	>133
	Celecoxib/enzyme-linked immunosorbent assay	3.7	0.06	61.7

Abbreviation: COX, cyclooxygenase.
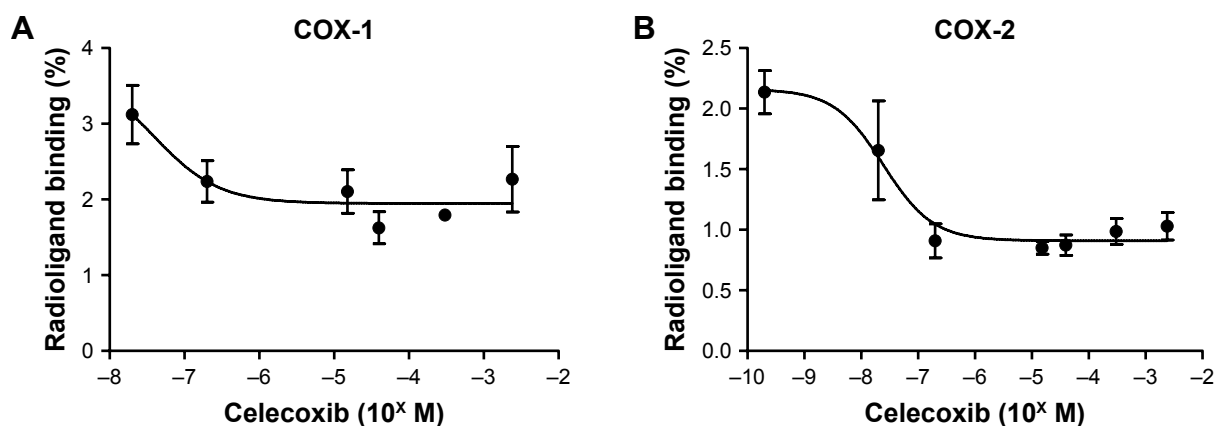
Figure 4 Plots of the formation of [¹⁸F]F–ligand–COX, *ortho*-[¹⁸F]F-**1**, in the presence of various concentrations of the competitor celecoxib (**A** and **B**).
Abbreviation: COX, cyclooxygenase.

These various concentrations were generated from a serial dilution from mother liquor. However, the lipophilic celecoxib limits the choice of solvents. The most concentrated sample comprises 3% dimethyl sulfoxide (DMSO) and the rest of the dilutions contain <1% DMSO. Also, the tracer sink was diluted with H_2O to lower DMSO concentration to <1/400. The toxic effect of DMSO is, therefore, negligible throughout both the tracer accumulation and the competitive inhibition studies. The two inhibition curves thus generated are interpolated to provide IC_{50} of 0.5 and 46.3 µM for COX-2 CCA and CCA, respectively. With a significant difference between the IC_{50} values of COX-2-overexpressed- and usual CCA cells, *ortho*-[¹⁸F]F-**1** was intended to trace those COX-2-overexpressed CCA tumors in vivo.

In vivo tracer accumulation studies for CCA tumor-bearing rats

To evaluate the specificity of the tagged ligand toward tumor loci, PET was coupled with *ortho*-[¹⁸F]F-**1** for CCA rats (n=4)
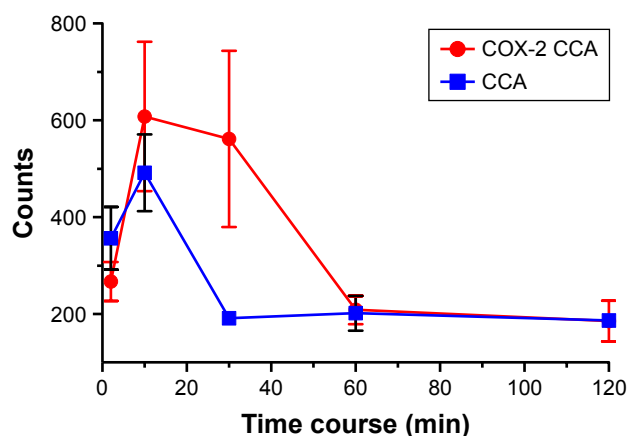

Figure 5 Tracer uptake of *ortho*-[¹⁸F]F-**1** in the COX-2-overexpressed murine CCA tumor cells and the murine CCA tumor cells as a control.
Abbreviations: CCA, cholangiocarcinoma; COX, cyclooxygenase.

and normal rats (n=2). The tumor loci was previously localized by PET with [¹⁸F]FDG (Figure 7A). Induction of CCA through administering thioacetamide (TAA) has been well characterized.[35] Oral administration of TAA in drinking water to male Sprague Dawley (SD) rats results in a multistep model of biliary dysplasia and invasive CCA, which closely mimics human CCA. The development is fairly reproducible using this carcinogenesis model, with a 50% yield rate of invasive CCA by the 16th week; by the 22nd week, the yield of invasive CCA is 100%. The PET studies were initially performed using a dynamic mode from 0 to 60 min with a 10-min period to acquire the temporal profile of these tagged compounds at the region of interest (ROI). Thus, an optimal scanning period was determinable for subsequent static study. Along with the half-life ($t_{1/2}$=30 min) and the sufficient number of animals for statistical comparison, systematic PET scans were established with the static mode from 30 to 60 min postinjection. Thus, the activity–time curves for *ortho*-[¹⁸F]F-**1** were derived from a plot of the intensity of the circled ROIs obtained from the PET images vs time, as shown in Figure 7B and C. The steady accumulation of *ortho*-[¹⁸F]F-**1** over the 1-h dynamic scanning period may indicate its selective uptake by COX-associated tumor cells followed by different release rates from the intracellular compartment to the extracellular compartment. The higher uptake ratio of [¹⁸F]FDG, which ranged between 2.2 and 2.4 (T/N), might be due to a longer circulation time that eliminated the background signals. In addition to inflammation-mediated accumulation, the formation of [¹⁸F]FDG-6-phosphate may assist its intracellular entrapment.[36]

In vivo tracer blocking studies for CCA tumor-bearing rats

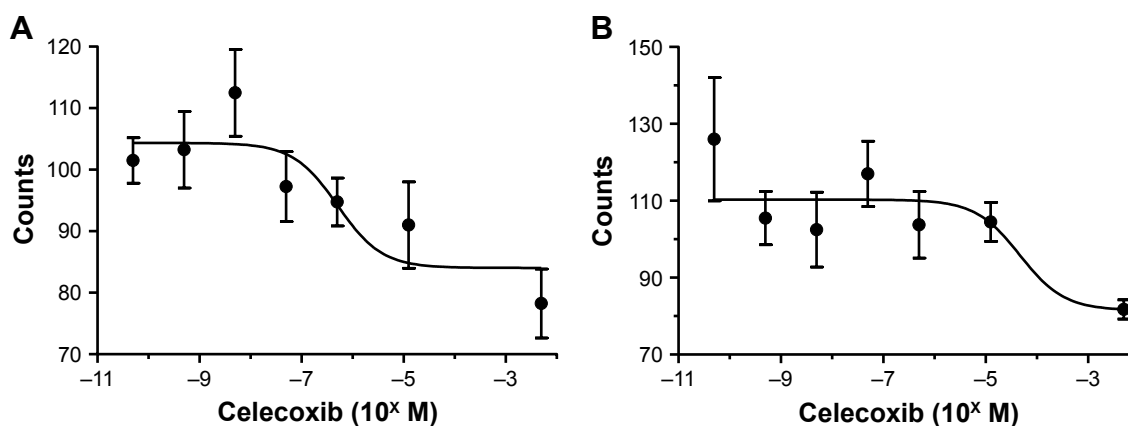The in vivo binding specificity of a tagged compound is commonly assessed using a PET approach.[37,38] We performed a

Figure 6 Competitive inhibition of the tracer accumulation (*ortho*-[^{18}F]F-**1**) in the presence of various concentrations of celecoxib (0.05 nM~250 μM).
Notes: In vitro system included COX-2-overexpressed CCA cells (**A**) and CCA cells (**B**). IC_{50}=0.5 and 46.3 μM for COX-2-overexpressed CCA and usual CCA cells, respectively.
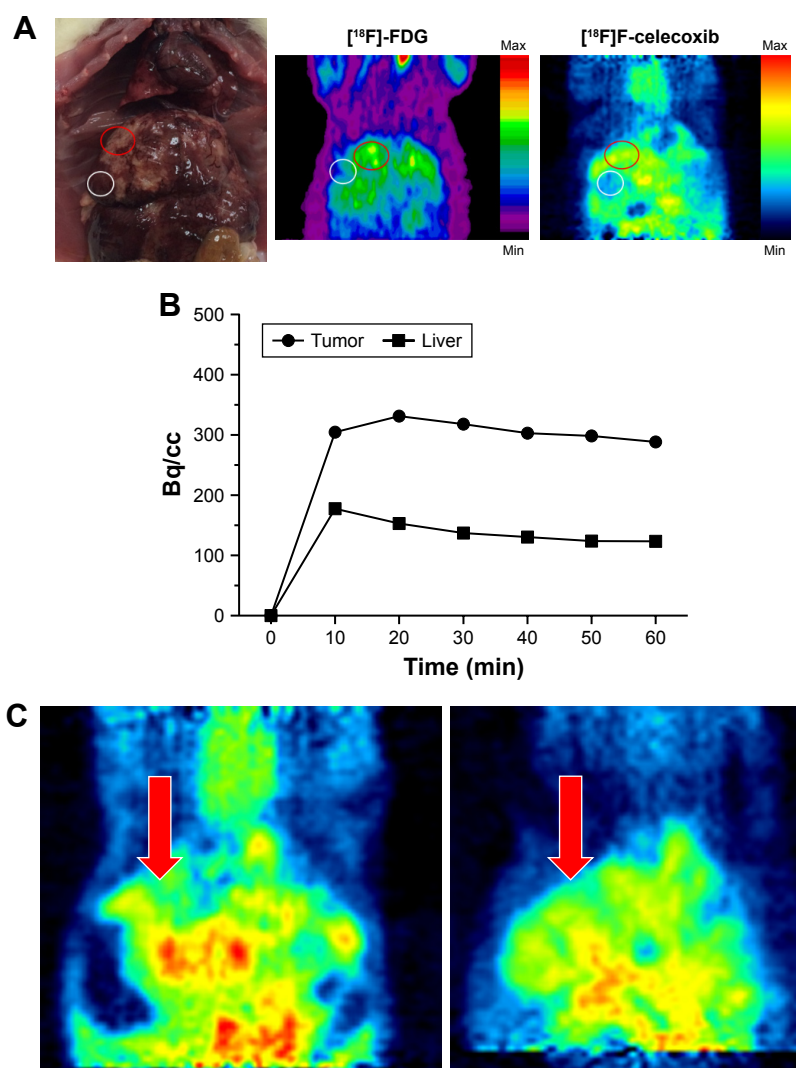**Abbreviations:** CCA, cholangiocarcinoma; COX, cyclooxygenase.

Figure 7 (**A**) Selected PET images taken of two F18-tagged ligands in the same.
Notes: Data for [^{18}F]FDG were obtained by scanning 90–120 min after intravenous injection into the tail vein. Data for *ortho*-[^{18}F]F-**1** were obtained by scanning 30–60 min postinjection. The red circles and white circles indicate the tumor loci and normal liver, respectively. (**B**) Activity–time curves of *ortho*-[^{18}F]F-**1** were constructed by counting the ROIs at the liver tumor loci and the adjacent normal region of the liver vs the scanning time over 1 h at 10-min intervals. (**C**) Dynamic PET studies of *ortho*-[^{18}F]F-**1** exemplified by coronal slices encompassing the liver of a CCA rat (left) and a normal rat (right) taken at 30–40 min in a 1-h scan. Red arrow bars indicate the ROIs circled for the tumor lesion (left) and the corresponding normal region (right), respectively. Number of rats used for the PET studies include n=4 for CCA rats and n=2 for normal rats.
Abbreviations: CCA, cholangiocarcinoma; PET, positron emission tomography; ROIs, regions of interest.
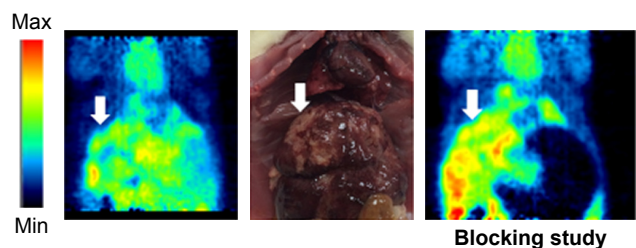
Figure 8 A representative comparison between the static PET images of *ortho*-[¹⁸F]F-**1** in a CCA rat (left) and in the same rat using cold celecoxib (2 mg) as a blocker (right).
Notes: The white arrows in a gross picture (middle) and in the two PET images indicate the tumor loci. The stronger signals in the PET images are comparable to the tumor lesions in the gross picture. The representative tumor grew in the upper-right lobe of liver. The blocking study using cold celecoxib did not result in signal reduction.
Abbreviations: CCA, cholangiocarcinoma; PET, positron emission tomography.

comparative study using CCA rats treated with four doses ranging from 1 to 4 mg and using one normal rat treated with a dose of 4 mg. Mixtures of *ortho*-[¹⁸F]F-**1** with different doses of celecoxib were coinjected to the rats per tail vein. Figure 8 represents a typical example of the obtained images. The results demonstrated a concentration dependency in the range of 1–3 mg of celecoxib (Table 2). However, marked variance was observed in the doses of 0 and 4 mg. The metabolism may be different between CCA rats and subsequently biasing the result (Figure 9). Because of the limited aqueous solubility, the relatively nontoxic solvent DMSO was used for dissolution. Therefore, to ensure animal survival, the maximal dose was limited to 4 mg, which may produce insignificant blocking.

To summarize the results, ROIs circled in 13 normal liver regions derived from eight rats, including CCA rats and normal rats, and blocking experiments for both, were compared with the ROIs circled in nine tumor regions derived from five CCA rats and blocking experiments. The tracer uptake by tumor and normal tissues was 1.16 ± 0.07 (%ID/g) and 0.87 ± 0.04 (%ID/g), respectively (Figure 10).

Conclusion

The radiofluoro analog of the selective COX-2 inhibitor celecoxib, *ortho*-[¹⁸F]F-**1**, was prepared using electrophilic fluorination. Through the direct binding assay of *ortho*-[¹⁸F]F-**1** with

COX-1 and COX-2 enzymes, submicromolar inhibition with slight COX-2 selectivity (1.63) was obtained. These results were in good agreement with other reported data. The indirect assay analyzes the COX–POX coupled function but not restricting to the sole COX binding. It was hypothesized that COX-2 accommodates celecoxib better than that by COX-1. COX-2-overexpressed CCA tumor cells took up more *ortho*-[¹⁸F]F-**1** than that by CCA tumor cells from 10 to 60 min postincubation. Furthermore, COX-2-overexpressed CCA cells also showed higher specificity to *ortho*-[¹⁸F]F-**1** than that by the usual CCA cells in an IC_{50} of 0.5 and 46.3 µM, respectively. PET studies of *ortho*-[¹⁸F]F-**1** showed slightly higher uptake in CCA tumor compared with normal liver (1.16%ID/g vs 0.87%ID/g). The substrate accumulation in tumor cell is correlated with the initial COX recognition. However, the subsequent POX function may not play a significant role in the tumor metabolism. Hence, this may explain the moderate selectivity of *ortho*-[¹⁸F]F-**1** (1.38 ± 0.12, T/N) in vivo, whereas the in vitro binding data are even better. The lipophilicity of *ortho*-[¹⁸F]F-**1** may increase its nonspecificity, and among which, carbonic anhydrase is the main enzyme responsible for this side effect.[39,40] Induction and maintenance of a constant concentration of COX-2 may play a role in the therapeutics of celecoxib.

Experimental
Preparation of 4-(5-(3-fluoro-4-methylphenyl)-3-(trifluoromethyl)-1H-pyrazol-1-yl)benzenesulfonamide (*ortho*-[¹⁸F]F-**1**)
Hot synthesis
A bottle of gas containing a mixture of F_2/Ne (0.9%) was used to fill an Al target chamber with a volume of 750 cm³ to attain a pressure of 9.12 atm (134 psi), equivalent to 2.8 mmol of F_2. Following bombardment with a beam line of deuterium of 8.5 MeV using an electric current of 40 µA for 2 h, the generated ¹⁸F-F_2 gas was passed through a cartridge (5.6×35 mm) packed with a KOAc/HOAc (1:1.5) powder.[25] The volatile mixture CH_3COOF/[¹⁸F]CH_3COOF (bp: 53°C) derived from the eluent (120 mCi) was bubbled through a solution of celecoxib (20 mg) (Matrix Scientific Co., Columbia, SC, USA) in trifluoroacetic acid (4 mL) for

Table 2 Comparison between the blocking studies of CCA rats and normal rats in the presence of a competitor, celecoxib, at various doses

Pharmacokinetics	CCA rat (n=5)		Normal rat (n=3)	
	ortho-[¹⁸F]F-**1**	*ortho*-[¹⁸F]F-**1**+ celecoxib (1–4 mg)	[¹⁸F]F-**1**	*ortho*-[¹⁸F]F-**1**+ celecoxib (4 mg)
T/N ratio	1.38 ± 0.23	1.48 ± 0.20		
Uptake (%ID/g)	1.14 ± 0.25	1.18 ± 0.22	0.99 ± 0.13	0.98

Abbreviations: CCA, cholangiocarcinoma; T/N ratio, tumor-to-normal ratio.
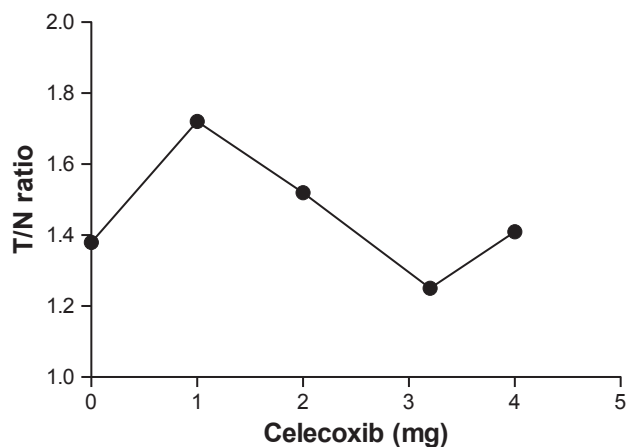
Figure 9 The dose–response curve for the CCA rats in the presence of the competitor celecoxib.
Abbreviations: CCA, cholangiocarcinoma; T/N ratio, tumor-to-normal ratio.

25 min. The mixture was then concentrated under reduced pressure at 42°C for 2 min, 52°C for 2 min, and 65°C for 10 min to obtain an almost dry residue (0.1 mL). After mixing with aqueous 85% CH_3CN (1.2 mL) for 2 min, the solution was passed through a 0.45 μm filter, and the filtrates were combined in a vial. The above procedure was repeated twice with aqueous 85% CH_3CN (1.2 mL), and the two filtrates were combined in a new vial. An activity of 35.9 mCi in a volume of 2.2 mL was obtained 60 min postreaction. The complete mixture was subjected to HPLC purification with a flow rate of 3 mL/min using 70% EtOH (aq). The desired fraction at t_R=19.97 min was collected. The isolated fraction was further identified with respect to its purity by using an analytic HPLC system. The retention time of 7.80 min corresponds to 99.92% radiochemical purity. After concentration under reduced pressure at 70°C, the obtained residue was mixed with DMSO (0.3 mL) and transferred to a plastic tube (3 mL).
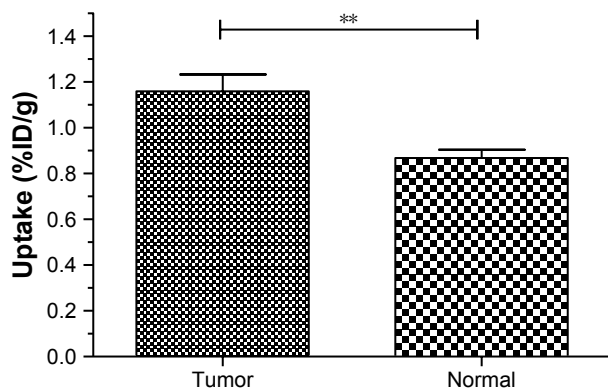

Figure 10 Comparison between the tracer uptake of *ortho*-[^{18}F]F-**1** in the tumor lesion of CCA rats (n=5) and normal liver region of the rats including CCA rats (n=13), P=0.0021, one-tailed Student's *t*-test. **The statistical variation is $p<0.005$.
Abbreviation: CCA, cholangiocarcinoma.

The mixing and transferring procedure was repeated three times, and further washes with saline (0.1 mL×4) and DMSO (0.1 mL) were carried out. The total wash volume (~1.5 mL) was combined in a tube as a stock for subsequent animal PET tests and radioligand-binding assays. A radiochemical yield of 9% (10.5 mCi) was obtained from the starting radioactive mixture (120 mCi) after 2 h and 10 min of decay correction (end of synthesis). An appropriate volume (0.1–0.3 mL) of the stock solution in a mixture of DMSO/saline (10:4) was drawn for each PET study to ensure a dosage of 0.6 mCi.

Cold synthesis of *ortho*-F-**1**

The same procedure was as described for *ortho*-[^{18}F]F-**1**, except for the radioactivity. The subsequent nonradioactive experiment was conducted in a chemical hood. The white residue was further treated twice with toluene (3 mL) to remove the volatile solvents. A mixture of *ortho*-F-**1** was obtained with a total yield of 10% (4 mg); according to the ^{1}H-NMR integral ratios, the desired product *ortho*-F-**1** constituted a yield of 8%. The sample was analyzed using ^{1}H-, ^{13}C-, and ^{19}F-NMR as well as low-resolution and high-resolution electrospray ionization mass spectrometry (ESI-MS). The original spectra were shown in "Supplementary spectroscopic data" (Supplementary materials) ^{1}H-NMR of *ortho*-F-celecoxib **1**, "Supplementary spectroscopic data" (Supplementary materials) ^{13}C-NMR (DEPT-135) of *ortho*-F-celecoxib **1**, "Supplementary spectroscopic data" (Supplementary materials) ^{19}F-NMR of *ortho*-F-celecoxib **1**, "Supplementary spectroscopic data" (Supplementary materials) LR ESI-MS of *ortho*-F-celecoxib **1**, and "Supplementary spectroscopic data" (Supplementary materials) HR ESI-MS of *ortho*-F-celecoxib **1**. The following masses were calculated for $C_{17}H_{13}F_4N_3O_2S$, [M+H]$^+$ (m/z): 400.07 (100.0%), 401.08 (18.4%), 402.07 (4.5%); [M+Na]$^+$ (m/z): 422.06 (100.0%), 423.06 (19.4%), 424.05 (4.5%); [2M+Na]$^+$=821.12 (100%), 822.13 (37.2%); found ESI+Q-TOF, [M+H]$^+$=400.07 (8.5%), 401.08 (1.7%); [M+Na]$^+$=422.05 (56.6%), 423.06 (9.1%), 424.05 (1.7%); and [2M+Na]$^+$=821.12 (5.5%), 822.12 (1.7%). For HRMS-ESI, calculated [M+H]$^+$=400.0743; found [M+H]$^+$=400.0741. ^{1}H-NMR (500 MHz, CDCl$_3$) δ 2.23 (d, $^4J_{HF}$=1.5 Hz, 3H, –CH$_3$, F-cel.), 2.31 (s, 3H, –CH$_3$, Cel.), 4.89 (s, 2H, –NH$_2$, F-cel.), 4.91 (s, 2H, –NH$_2$, Cel.), 6.67 (s, 1H, arom., F-cel.), 6.69 (s, 1H, arom., Cel.), 6.79 (dd, $J_{5'',6''}$=8.0, $J_{5'',F}$=2.0 Hz, 1H, arom., 5''-H, F-cel.), 6.84 (dd, $^3J_{2'',F}$=10.0, $J_{2'',6''}$=1.5 Hz, 1H, arom., 2''-H, F-cel.), 7.04 (d, J=8.0 Hz, 2H, arom., Cel.), 7.11 (d, J=8.0 Hz, 2H, arom., Cel.), 7.12 (d, $J_{6'',5''}$=8.0 Hz, 1H, arom., Cel., 6''-H, F-cel.), 7.39–7.42 (m, 2H, arom., Cel.+F-cel.), 7.82–7.87 (m, 2H, arom., Cel.+F-cel.). ^{13}C-NMR (125 MHz, CDCl$_3$) δ 14.46 (d, $^3J_{CF}$=3.2 Hz, CH$_3$, F-cel.),

106.37 (CH, arom., Cel.), 106.70 (CH, arom., F-cel.), 115.40 (d, J_{CF}=24.2 Hz, CH, arom., F-cel.), 116.58 (q, $^1J_{CF}$=293.8 Hz, CF_3), 124.35 (d, $^4J_{CF}$=3.1 Hz, CH, arom., F-cel.), 124.60 (CH, arom., F-cel.), 124.74 (s, CH, arom., Cel.), 126.84 (d, $^2J_{CF}$=16.7 Hz, C, arom., F-cel.), 127.50 (CH, arom., Cel.), 127.62 (CH, arom., F-cel.), 127.76 (d, $^3J_{CF}$=8.2 Hz, C, arom., F-cel.), 132.22 (d, $^3J_{CF}$=5.5 Hz, CH, arom., F-cel.), 138.08 (C, arom., F-cel.), 139.81 (C, arom., Cel.), 141.27 (C, arom., Cel.), 141.59 (C, arom., F-cel.), 142.28 (C, arom., Cel.), 142.59 (C, arom., Cel.), 144.05 (q, $^2J_{CF}$=38.5 Hz, C, CCF$_3$), 161.11 (d, $^1J_{CF}$=245.8 Hz, C, arom., F-cel.). ^{19}F-NMR (470 MHz, CDCl$_3$)δ −62.50 (s, CF$_3$), −115.06 (s, arom.).

Radioligand-binding assay

An aliquot of COX-1 (80 µL, 1,600 units), COX-2 (200 µL, 1,560 units), or *m*-prostaglandin E synthase (125 µL, 275 units) was drawn from each of the respective commercial products and added to a plastic tube. Volumes of 1,920, 1,800, and 220 µL of Tris buffer (0.1 M, pH=8.0) were added to obtain a working concentration equivalent to 68 units/85 µL. A volume of 85 µL/well of the stock solution was added to a 96-well microtiter plate, followed by addition of the competitor celecoxib (10 µL) at concentrations of 0.002, 0.2, 2, 150, 400, 3,000, and 24,000 µM to yield a 10-fold dilution to produce final concentrations of 0.0002, 0.02, 0.2, 15, 40, 300, and 2,400 µM, respectively. The radiotracer solution of *ortho*-[18F]F-**1** was prepared as a stock solution in EtOH (2×10^6 Bq/mL) obtained from the desired fractions after HPLC purification, and 5 µL (10,000 Bq) was added to each well. After standing for 10 min, the mixture in each well was transferred through pipette to a silica cartridge (Sep-Pak; Waters, Milford, MA, USA) followed by pumping through a blood pressure ball. The procedure was repeated by adding another portion of EtOH (0.5 mL). The two eluted portions were combined. The cartridge and filtrates were individually counted using an autogamma counter. The counts from both phases were used to deduce the binding percentage from the formula: counts (solid)/[counts (solid)+counts (effluents)]×100 (%). The displacement binding curve was obtained from a plot of the binding percentage vs the concentration of *ortho*-F-**1** GraphPad Software, Inc., La Jolla, CA, USA). The IC$_{50}$ value for the displacement binding of *ortho*-[18F]F-**1** to COXs in the presence of celecoxib was obtained through manual adjustment. All experiments were performed in triplicate.

In vitro tracer uptake assay

Tracer uptake of *ortho*-[18F]F-**1** was performed using COX-2-overexpressed CCA cells and usual CCA cells. Preparation of CCA cells has been reported earlier.[33] The COX-2 expression pCDNA3 plasmid was obtained as a gift from Shyue, Song-Kun Lab, Institute of Biomedical Sciences, Academia Sinica, Taipei, Taiwan. The transfection with COX-2 expression pCDNA3 plasmid using lipofectamine (Thermo Fisher Scientific, Waltham, MA, USA) was according to the manual protocol and selected by Geneticin (Thermo Fisher Scientific). The concentrate of *ortho*-[18F]F-**1** generated from hot synthesis (3–5 mCi) was diluted to 1 mL using DMSO. An aliquot of 0.2 mCi was mixed with 20 mL of H$_2$O in a polypropylene-based reservoir as shown in Figure S1 and Table S1. The two cells were seeded in a 96-well microtiter plate as a population of 10,000 per each well. An aliquot of 20 µL was transferred to each of the wells through a multichannel pipette, and the plate was placed on a water bath at 37°C. After various time points, the medium of each of the corresponding wells was removed, and 200 µL of distilled water was added for washing the residual medium. All the media were discarded. At 2 h postreaction, the cell pellets from all time points were detached by using 200 µL of 4N HCl (aq.), and the mixture each was transferred to a counting tube. After addition of H$_2$O (2 mL), these tubes along with those tubes of in vitro blocking tests as described subsequently were counted by using a gamma counter made by 2470 Automatic Gamma Counter (PerkinElmer Inc., Waltham, MA, USA). The data were obtained in quadruple.

In vitro tracer blocking assay

A mother liquor of 50 mM of celecoxib in DMSO (2 mL) was first prepared in an Eppendorf tube. After dilution of an aliquot of 0.2 mL with 1.8 mL of aqueous DMSO (60%, v/v), the most concentrated competitor celecoxib (5 mM) was obtained. The subsequent serial dilution using H$_2$O in 10–25-fold gave the next six samples, sequentially, with concentrations of 250 µM, 10 µM, 1 µM, 100 nM, 10 nM, and 1 nM. Each of the seven samples (100 µL) and *ortho*-[18F]F-**1** (100 µL), derived from 0.2 mCi in 20 mL of H$_2$O, were mixed in a polypropylene-based 96-well plate as shown in Figure S2 and Table S2. An aliquot of 20 µL of the mixture was transferred to each well of a cell-seeded 96-well microtiter plate, as described earlier. The concentration of celecoxib in the well of the plate was automatically diluted to 20-fold based on the presence of 200 µL of medium corresponding to 250 µM, 12.5 µM, 0.5 µM, 50 nM, 5 nM, 0.5 nM, and 0.05 nM. After standing at 37°C for 10 min, multiple mediums were removed using a multichannel pipette. The subsequent washing and removal of the attached cell pellets followed the same procedure as that described for tracer accumulation protocol. The data were obtained in quadruple.

Rat model

All in vivo experiments were conducted in compliance with the NHMRC Taiwan Code of Practice for the care and use of animals for scientific purposes[41] and the Animal Use Protocols of Chang Gung Memorial Hospital. The study was approved by the Institutional Animal Care and Use Committee of Chang Gung Memorial Hospital (No 2013092702) and the Institutional Animal Care and Use Committee of Chang Gung University (No CGU12-055). Male SD rats aged 49 weeks were obtained from the Animal Research Center at Chang-Gung Memorial Hospital, Taiwan. The rats were housed under fixed environmental conditions and had free access to food and water throughout the experimental period.

Animals were fed regularly after recovery from anesthesia. They were carefully monitored with respect to the feeding quality, interaction, and symptoms of dystrophy. The animal care unit checked for abnormalities such as a feeding intake ratio <50% in 72 h, hind leg paraparesis, or a weight loss >20%. If the abovementioned situations occurred, the animal was sedated with isoflurane and xylazine hydrochloric acid and euthanized by CO_2 and intravenous xylocaine (200 mg).

Induction of CCA through administering TAA has been well characterized.[35] Briefly, oral administration of TAA in drinking water to male SD rats results in a multistep model of biliary dysplasia and invasive CCA, which closely mimics human disease. Similar to preneoplastic lesions described in human CCAs, the rat cholangiolar epithelium displays a phase of progressive "biliary dysplasia" preceding invasive cancer. In addition, both the precancerous and neoplastic biliary epithelia demonstrate foci of intestinal metaplasia (goblet cells), another well-known feature of the human counterpart. The strong, diffuse expression of biliary cytokeratin (CK19) confirms the bile ductular ontogeny of the neoplastic cells. The course of events is fairly reproducible using this carcinogenesis model, with a 50% yield rate of invasive CCA by the 16th week; by the 22nd week, the yield of invasive CCA is 100%. Notably, the occurrence of biliary dysplasia and invasive CCA precedes the development of hepatic fibrosis by 4 weeks, arguing against a "secondary" biliary proliferation in response to cirrhosis.

Small-animal PET imaging study of *ortho*-[18F]F-1

In vivo PET studies of *ortho*-[18F]F-1 were performed using TAA-induced CCA rats (n=5 at 37 weeks postadministration) and using normal rats as a control (n=3).[32,35] These studies were performed at Taipei VGH. The rats were anesthetized through isoflurane inhalation (Forthane; Abbott Laboratories, Abbott Park, IL, USA) in oxygen (200 mL/min) during the imaging study.

A RODENT microPET R4 scanner (Concorde Micro-systems Inc., Knoxville, TN, USA) was used for the small-animal PET scanning study. The crude data generated from the PET study were further processed using the Preclinical Multi-Modality Data Analysis software (ver 3.2; PMOD Technologies Ltd, Zurich, Switzerland).

For the dynamic PET study of *ortho*-[18F]F-1 (one CCA rat and one normal rat), the rats were first anesthetized with 3%–4% isoflurane, and the liver was positioned in the center of the field of view. After injection of 22.2±1.0 MBq of *ortho*-[18F]F-1 through the tail vein, a 1-h dynamic PET scan was performed to collect 10-min frames six times for each animal. The 10-min frames were either analyzed directly or binned together to obtain a 30–60-min scanning set. The six frames were used to plot activity–time curves with respect to the ROIs covering either the tumor sites or the adjacent normal regions vs the time course. The binned data sets from frame 4 to frame 6 could additionally serve as one static image frame (30–60 min). The static imaging mode was obtained from the imaging data over 30–60 min postinjection for both the tracer distribution study of CCA rats (n=4) and normal rats (n=2) and the blocking study of CCA rats (n=4) and normal rats (n=1). As described in the next section, the PET studies encompassed three normal rats and five CCA rats. The obtained images were reconstructed using two-dimensional ordered subset expectation maximization (OSEM 2D) and processed by PMOD 3.2 imaging analysis software. ROIs were drawn over the tumor with a threshold (maximum intensity minus minimum intensity)×50% and over the normal liver region. The average intensity in the ROIs was measured. Assuming a tissue density of 1 g/cm^3, the unit of the ROIs (kBq/cm^3) was converted to microcuries per gram and then divided by the administered activity to obtain an image ROI-derived percentage of the injected dose per gram of tissue (%ID/g).

PET study of *ortho*-[18F]F-1 in the presence of the blocking agent, celecoxib

Considering the limited aqueous solubility of *ortho*-[18F]F-1 and the toxicity of DMSO used to enhance the solubility, a maximal dosage of 4 mg of celecoxib was used in the blocking experiment. Doses of 1, 2, 3.4, and 4 mg of celecoxib were used. Mixing of the *ortho*-[18F]F-1 with various doses of celecoxib were then injected into CCA or normal rats. The static PET imaging studies were performed accordingly.

Author contributions

All authors contributed toward data analysis, drafting and revising the paper and agree to be accountable for all aspects of the work. All authors contributed toward data analysis, drafting and revising the paper and agree to be accountable for all aspects of the work.

Disclosure

The authors report no conflicts of interest in this work.

References

1. Hayashi N, Yamamoto H, Hiraoka N, et al. Differential expression of cyclooxygenase-2 (COX-2) in human bile duct epithelial cells and bile duct neoplasm. *Hepatology*. 2001;34(4):638–650.
2. Sirica AE, Lai GH, Zhang ZC. Biliary cancer growth factor pathways, cyclo-oxygenase-2 and potential therapeutic strategies. *J Gastroenterol Hepatol*. 2001;16(4):363–372.
3. Sirica AE, Lai GH, Endo K, Zhang ZC, Yoon BI. Cyclooxygenase-2 and ERBB-2 in cholangiocarcinoma: potential therapeutic targets. *Semin Liver Dis*. 2002;22(3):303–313.
4. Marks EI, Yee NS. Molecular genetics and targeted therapeutics in biliary tract carcinoma. *World J Gastroenterol*. 2016;22(4):1335–1347.
5. Bridgewater J, Galle PR, Khan SA, et al. Guidelines for the diagnosis and management of intrahepatic cholangiocarcinoma. *J Hepatol*. 2014; 60(6):1268–1289.
6. Taylor-Robinson SD, Toledano MB, Arora S, et al. Increase in mortality rates from intrahepatic cholangiocarcinoma in England and Wales 1968–1998. *Gut*. 2001;48(6):816–820.
7. Khan SA, Taylor-Robinson SD, Toledano MB, Beck A, Elliott P, Thomas HC. Changing international trends in mortality rates for liver, biliary and pancreatic tumours. *J Hepatol*. 2002;37(6):806–813.
8. Casavilla FA, Marsh JW, Iwatsuki S, et al. Hepatic resection and transplantation for peripheral cholangiocarcinoma. *J Am Coll Surg*. 1997;185(5):429–436.
9. Ohtsuka M, Ito H, Kimura F, et al. Results of surgical treatment for intrahepatic cholangiocarcinoma and clinicopathological factors influencing survival. *Br J Surg*. 2002;89(12):1525–1531.
10. Smith WL, Urade Y, Jakobsson PJ. Enzymes of the cyclooxygenase pathways of prostanoid biosynthesis. *Chem Rev*. 2011;111(10):5821–5865.
11. Khan SA, Davidson BR, Goldin RD, et al. Guidelines for the diagnosis and treatment of cholangiocarcinoma: an update. *Gut*. 2012;61(12):1657–1669.
12. Sirica AE. Cholangiocarcinoma: molecular targeting strategies for chemoprevention and therapy. *Hepatology*. 2005;41(1):5–15.
13. Berthiaume EP, Wands J. The molecular pathogenesis of cholangiocarcinoma. *Semin Liver Dis*. 2004;24(2):127–137.
14. Burr NE Talboys RJ, Savva S, et al. Aspirin may prevent cholangiocarcinoma: a case-control study from the United Kingdom. *Digest Dis Sci*. 2014;59(7):1567–1572.
15. Jendrossek V. Targeting apoptosis pathways by Celecoxib in cancer. *Cancer Lett*. 2013;332(2):313–324.
16. Preshlock S, Tredwell M, Gouverneur V. F-18-labeling of arenes and heteroarenes for applications in positron emission tomography. *Chem Rev*. 2016;116(2):719–766.
17. Prabhakaran J, Underwood MD, Parsey RV, et al. Synthesis and in vivo evaluation of F-18 -4- 5-(4-methylphenyl)-3-(trifluoromethyl)-1H-pyrazol-1-yl benzene sulfonamide as a PET imaging probe for COX-2 expression. *Bioorg Med Chem*. 2007;15(4):1802–1807.
18. Toyokuni T, Kumar JSD, Walsh JC, et al. Synthesis of 4-(5-F-18 fluoromethyl-3-phenylisoxazol-4-yl)-benzenesulfonamide, a new F-18 fluorinated analogue of valdecoxib, as a potential radiotracer for imaging cyclooxygenase-2 with positron emission tomography. *Bioorg Med Chem Lett*. 2005;15(21):4699–4702.
19. Uddin MJ, Crews BC, Ghebreselasie K, et al. Fluorinated COX-2 Inhibitors as Agents in PET Imaging of Inflammation and Cancer. *Cancer Prev Res*. 2011;4(10):1536–1545.
20. Riese J, Hoff T, Nordhoff A, Dewitt DL, Resch K, Kaever V. Transient expression of prostaglandin endoperoxide synthase-2 during mouse macrophage activation. *J. Leukoc Biol*. 1994;55(4):476–482.
21. McCarthy TJ, Sheriff AU, Graneto MJ, Talley JJ, Welch MJ. Radiosynthesis, in vitro validation, and in vivo evaluation of F-18-labeled COX-1 and COX-2 inhibitors. *J Nucl Med*. 2002:43(1):117–124.
22. de Vries EFJ, van Waarde A, Buursma AR, Vaalburg W. Synthesis and in vivo evaluation of F-18-desbromo-DuP-697 as a PET tracer for cyclooxygenase-2 expression. *J Nucl Med*. 2003;44(10):1700–1706.
23. Rini BI, Weinberg V, Dunlap S, et al. Maximal COX-2 immunostaining and clinical response to celecoxib and interferon alpha therapy in metastatic renal cell carcinoma. *Cancer*. 2006;106(3):566–575.
24. Fabi A, Metro G, Papaldo P, et al. Impact of celecoxib on capecitabine tolerability and activity in pretreated metastatic breast cancer: results of a Phase II study with biomarker evaluation. *Cancer Chemother Pharmacol*. 2008;62(4):717–725.
25. Jewett DM, Potocki JF, Ehrenkaufer RE. A gas solid-phase microchemical method for the synthesis of acetyl hypofluorite. *J Fluorine Chem*. 1984;24(4):477–484.
26. Biava M, Porretta GC, Poce G, et al. Cyclooxygenase-2 inhibitors. 1,5-diarylpyrrol-3-acetic esters with enhanced inhibitory activity toward cyclooxygenase-2 and improved cyclooxygenase-2/cyclooxygenase-1 selectivity. *J Med Chem*. 2007;50(22):5403–5411.
27. Husain A, Ahmad A, Alam MM, Ajmal M, Ahuja P. Fenbufen based 3- 5-(substituted aryl)-1,3,4-oxadiazol-2-yl -1-(biphenyl-4-yl)propan-1-ones as safer antiinflammatory and analgesic agents. *Eur J Med Chem*. 2009;44(9):3798–3804.
28. Hood WF, Gierse JK, Isakson PC, et al. Characterization of celecoxib and valdecoxib binding to cyclooxygenase. *Mol Pharmacol*. 2003; 63(4):870–877.
29. Gierse JK, Zhang Y, Hood WF, et al. Valdecoxib: assessment of cyclooxygenase-2 potency and selectivity. *J Pharmacol Exp Ther*. 2005; 312(3):1206–1212.
30. Huang HL, Yeh CN, Lee WY, et al. I-123 Iodooctyl fenbufen amide as a SPECT tracer for imaging tumors that over-express COX enzymes. *Biomaterials*. 2013;34(13):3355–3365.
31. Huang HL, Huang YC, Lee WY, Yeh CN, Lin KJ, Yu CS. F-18-glutathione conjugate as a PET tracer for imaging tumors that overexpress L-PGDS enzyme. *PLoS One*. 2014;9(8):14.
32. Yeh CN, Chang CW, Chung YH, et al. Synthesis and characterization of boron fenbufen and its F-18 labeled homolog for boron neutron capture therapy of COX-2 overexpressed cholangiocarcinoma. *Eur J Pharm Sci*. 2017;107:217–229.

33. Yeh CN, Lin KJ, Chen TW, et al. Characterization of a novel rat cho-langiocarcinoma cell culture model-CGCCA. *World J Gastroenterol*. 2011;17(24):2924–2932.

34. Chen SF, Wu CH, Lee YM, et al. Caveolin-1 interacts with derlin-1 and promotes ubiquitination and degradation of cyclooxygenase-2 via collaboration with p97 complex. *J Biol Chem*. 2013;288(46): 33462–33469.

35. Yeh CN, Maitra A, Lee KF, Jan YY, Chen MF. Thioacetamide-induced intestinal-type cholangiocarcinoma in rat: an animal model reca-pitulating the multi-stage progression of human cholangiocarcinoma. *Carcinogenesis*. 2004;25(4):631–636.

36. Monakhov NK, Neistadt EL, Shavlovskil MM, Shvartsman AL, Neifakh SA. Physicochemical properties and isoenzyme composition of hexokinase from normal and malignant human tissues. *J Natl Cancer Inst*. 1978;61(1):27–34.

37. Li ZB, Cai WB, Cao QZ, et al. 64Cu-labeled tetrameric and octameric RGD peptides for small-animal PET of tumor alpha(v)beta(3) integrin expression. *J Nucl Med*. 2007;48(7):1162–1171.

38. Jacobson O, Weiss ID, Kiesewetter DO, Farber JM, Chen XY. PET of tumor CXCR4 expression with 4-F-18-T140. *J Nucl Med*. 2010; 51(11):1796–1804.

39. Tietz O, Wuest M, Marshall A, et al. PET imaging of cyclooxygenase-2 (COX-2) in a pre-clinical colorectal cancer model. *EJNMMI Res*. 2016;6:11.

40. Weber A, Casini A, Heine A, et al. Unexpected nanomolar inhibition of carbonic anhydrase by COX-2-selective celecoxib: new pharmacologi-cal opportunities due to related binding site recognition. *J Med Chem*. 2004;47(3):550–557.

41. Chung YH, Hsu PH, Huang CW, et al. Evaluation of prognostic integrin alpha 2 beta 1 PET tracer and concurrent targeting delivery using focused ultrasound for brain glioma detection. *Mol Pharm*. 2014;11(11):3904–3914.